Thin Solid Films 518 (2009) 1566–1570

Contents lists available at ScienceDirect

Thin Solid Films

journal homepage: www.elsevier.com/locate/tsf

Modulated pulse power sputtered chromium coatings

Jianliang Lin [a], John J. Moore [a,*], William D. Sproul [a,b], Brajendra Mishra [a], Zhili Wu [a]

[a] Advanced Coatings and Surface Engineering Laboratory (ACSEL), Colorado School of Mines, Golden, Colorado, 80401, USA
[b] Reactive Sputtering, Inc., 2152 Goya Place, San Marcos, California, 92078, USA

ARTICLE INFO

Available online 6 October 2009

Keywords:
Modulated pulse power (MPP)
High power pulsed magnetron sputtering (HPPMS)
Cr coating
Ion bombardment
Adhesion

ABSTRACT

Cr coatings were deposited using continuous dc magnetron sputtering (dcMS) and modulated pulse power sputtering (MPP) techniques in a closed field unbalanced magnetron sputtering system at equivalent average target powers. It was found that MPP sputtering exhibited higher deposition rates than in dcMS when the average target power density was above 14 W cm^{-2} for the Cr coating depositions. Plasma diagnostics confirmed a significant increase in the numbers of both target material (Cr) and gas (Ar) ions in the MPP plasma as compared to the dc plasma. The substrate peak current densities measured in the MPP depositions (104–324 mA cm^{-2}) have been increased by over a factor of 50 to those in the dcMS conditions (2–5.5 mA cm^{-2}). The enhanced ion flux bombardment from the highly ionized MPP plasma led to the formation of denser microstructure and finer grain size in the MPP Cr coatings than in the dcMS Cr coatings. In addition, MPP sputtered Cr coatings exhibited improved hardness and adhesion.

Published by Elsevier B.V.

1. Introduction

As a novel ionized physical vapor deposition (I-PVD) technique, high power pulsed magnetron sputtering (HPPMS) (also known as high power impulse magnetron sputtering (HIPIMS)) was developed in the 1990s [1–4]. It creates a high density plasma of a high degree of ionization of the sputtered species using a pulsed high peak target power density (e.g. 1–3 kW cm^{-2}) for a short period of time (e.g. 5–150 μs). The HPPMS technique has been shown to improve the coating structure and properties [1,5,6], achieve uniform depositions [7,8], and enhance coating adhesion [9,10] as compared to continuous dc magnetron sputtering (dcMS). However, one downside of HPPMS technique is that the deposition rate is lower than the dc rate for an equivalent amount of average target power because the ions can be attracted back toward the target and captured by the negative potential on the cathode [11–13].

As an alternative HPPMS deposition technique, modulated pulse power (MPP) has been developed in recent years after the development of HPPMS/HIPIMS [14–16]. The MPP technique uses longer pulse lengths (up to 3 ms) than does HPPMS. In addition, MPP utilizes multiple steps and micro pulses in one pulse period. One typical MPP pulse consisting of two stages in one pulse is shown in Fig. 1. The first step is the weakly ionized period, in which low voltage, current and power are loaded on the target to ignite the plasma. Then the pulse goes to the strongly ionized period with high voltage, current and power. It should be noted that there can be multiple steps in one MPP pulse to reach the strong ionization period. By varying the pulsing width (up to 3000 μs), frequency (4 to 400 Hz), voltage 'on' time (τ_{on}) (the width of micro pulses) and the voltage 'off' time (τ_{off}) (the distance between micro pulses) in the micro pulses, MPP can generate controllable peak power (P_p) up to 360 kW, a maximum average target power (P_a) of 20 kW, and a maximum peak current (I_p) of 550 A on the target during the strong ionization segment.

In the present investigation, we report the results on the comparisons of the plasma properties, the deposition rate, and the structure and properties of Cr coatings deposited by sputtering of a metal Cr target in an Ar atmosphere using MPP and continuous dc power sources in a closed field unbalanced magnetron sputtering system.

2. Experimental details

Cr coatings were deposited from a metal Cr target (99.95%) using continuous dc (Pinnacle, Advanced Energy Inc.) and MPP power sources (Zpulser, LLC) in a closed field unbalanced magnetron sputtering system which is equipped with two Teer Coatings Ltd unbalanced magnetrons. The target size is 300 mm × 100 mm. The effective sputter area enclosed in the sputter track is 180 mm^2, which was used to calculate the average target power density (P_d) on the target. The working pressure was 0.4 Pa, and the Ar flow rate was kept constant at 30 sccm. AISI 304 stainless steel coupons and (100) Si wafers were used as the substrates, which were installed 140 mm away from the Cr target. The substrates were sputter etched using Ar^+ plasma bombardment at a −450 V bias prior to the depositions. A −50 V dc substrate bias was used for all depositions. Two pulse widths were used for the MPP sputtering: 750 and 1500 μs. The pulses begin with a 500 μs weakly ionized period followed by a strongly ionized period, as shown in Fig. 1. The pulse

* Corresponding author. Tel.: +1 303 273 3771; fax: +1 303 273 3795.
E-mail address: jjmoore@mines.edu (J.J. Moore).

0040-6090/$ – see front matter. Published by Elsevier B.V.
doi:10.1016/j.tsf.2009.09.118

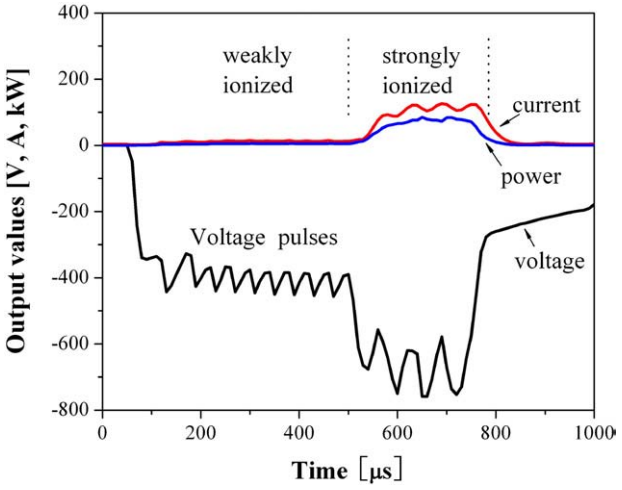

Fig. 1. The target voltage, current and power waveforms during one typical modulated pulse (total pulse width = 750 μs; τ_{off}/τ_{on} = 34/6 μs during the weak ionization stage; τ_{off}/τ_{on} = 6/10 μs during the strong ionization stage; pulsing frequency = 100 Hz).

frequency was fixed at 100 Hz for the 750 μs pulse, and 30 Hz for the 1500 μs pulse. The average target power and current were set at 4.5 kW and 12 A, respectively, during the weakly ionized period by using τ_{off} and τ_{on} at 34 and 6 μs respectively. During the strongly ionized period, MPP generated different P_p and I_p values on the target by varying τ_{on} in the micro pulses as summarized in Table 1. For the dcMS, the target power was regulated from 1 to 4 kW. The deposition time was 30 min for all depositions.

A Hiden Analytical Ltd electrostatic quadrupole plasma mass spectrometer (EQP) was used to characterize the ion mass distributions (IMD) in the plasma. The detailed configurations of the EQP probe and the deposition system and the plasma diagnostic procedures were presented in ref. [16]. The crystal structure of the coatings was studied using X-ray diffractometry (XRD) in the θ–2θ mode using Cu K_α(λ = 0.15406 nm) radiation. The thickness and microstructure of the coatings were examined using a JSM-7000F field-emission scanning electron microscope (SEM). The hardness of the coatings was measured by a nanoindenter (NanoIndenter XPTM, MTS Systems Corporation) equipped with a Berkovich diamond indenter using the depth sensing method from the load displacement curves taking 10% of the coating thickness as the effective indentation depth. A microstratch tester (CSM instruments, LLC) was used to evaluate the adhesion of the coatings using a Rockwell C indent tip (200 μm). The tests were carried out by progressively increasing the normal load from 0.03 to 30 N with a rate of 20 N min^{-1} and a scratch length of 3 mm. After the test, the scratch tracks were examined using the attached optical scope.

3. Results and discussion

3.1. Properties of the MPP and dc plasmas

A comparison of the IMDs in the dc and MPP plasmas for sputtering of a Cr target in the pure Ar at a P_a of 4 kW is shown in Fig. 2. The IMDs were scanned at an ion energy of 5 eV for the dcMS and MPP plasmas. The intensity of the metal Cr^+ ions is low as compared to the gas Ar^+ ions in the dc plasma, indicating a low target material ionization degree. On the other hand, significantly increased numbers of Cr^+ and Ar^+ ions were identified in the MPP plasma generated at the same P_a but with a P_p of 135 kW and an I_p of 189 A, confirming that a large fraction of the target Cr atoms was ionized in the MPP plasma due to the high P_p and I_p on the target. A more detailed study of the MPP and dc plasma properties can be found in ref. [16].

3.2. Deposition rates of MPP and dcMS sputtered Cr coatings

Fig. 3 shows the deposition rates of dcMS and MPP Cr coatings as a function of the P_d. For dcMS, the deposition rate increased almost linearly as the P_d was increased from 5.6 to 19.4 W cm^{-2}. The deposition rates of Cr coatings in MPP are lower than the dcMS rates when the P_d is less than 14 W cm^{-2}. However, the MPP deposition rates exceeded the dcMS deposition rates as the P_d is higher than 14 W cm^{-2}. The reasons for the increased deposition rate with MPP need further investigations, but it is proposed that the high rate is due to both sputtering and evaporation/sublimation processes taking place on the target surface at a high target power and current [17].

3.3. Microstructure of MPP and dcMS sputtered Cr coatings

Figs. 4 and 5 show the XRD patterns of dcMS and MPP Cr coatings deposited at similar P_a values respectively. The cross-sectional and top view SEM micrographs of the coatings were inserted in the figures. As shown in Fig. 4, dcMS Cr coatings exhibited a strong body center cubic (bcc) Cr (110) peak when the target power was less than 2 kW. A change of the preferred orientation from (110) to (200) was observed as P_a was increased to above 3 kW. A significant increase in the grain size (~1 μm) of the dcMS Cr coatings deposited at 3 and 4 kW target powers was observed. An increase in the target power in dcMS will increase the energy of the particles but it will also decrease the ion to neutral ratio at higher target powers [18]. The decreased ion to neutral ratio will decrease the energy deposited per atom on the

Table 1
Pulsing parameters and deposition conditions for the Cr coating depositions using MPP and dcMS power sources.

Sample ID	Pulsing parameters				Deposition conditions									Hardness [GPa]	Thickness [μm]
	τ_{total} [μs]	$\tau_{weak}/\tau_{strong}$ [μs]	τ_{off}/τ_{on} [μ s]	f	P_a [kW]	P_p [kW]	V_a [V]	V_p [V]	I_a [A]	I_p [A]	I_d [A cm^{-2}]	I_{sub} [mA cm^{-2}]	T_{sub} [°C]		
C1	750	500/250	6/8	100	1.2	43	495	742	25	70	0.4	104.5	145	9.3 ± 0.26	2.2
C2	750	500/250	6/10	100	1.6	65	500	817	33	94	0.5	148.5	193	9.5 ± 0.50	2.7
C3	750	500/250	6/12	100	2.1	90	495	829	42	122	0.6	210.2	227	10.4 ± 0.85	3.1
C4	750	500/250	6/16	100	2.8	125	494	882	53	174	0.8	262.7	293	12.8 ± 0.68	4.8
C5	1500	500/1000	6/16	30	4.0	135	664	847	114	189	1.1	324.8	356	15.2 ± 0.82	6.9
dc-1	N/A				1.0	1.0	402	402	2.5	2.5	0.01	2.1	183	8.2 ± 0.56	2.0
dc-2					1.6	1.6	429	429	3.7	3.7	0.02	2.9	245	8.0 ± 0.69	2.8
dc-3					2.0	2.0	431	431	4.6	4.6	0.02	3.5	268	6.7 ± 0.89	3.6
dc-4					3.0	3.0	477	477	6.3	6.3	0.03	4.3	354	4.5 ± 1.11	4.2
dc-5					4.0	4.0	500	500	8.0	8.0	0.04	5.5	377	4.3 ± 0.96	4.9

(1) τ_{total}: total pulse width for one pulse; (2) $\tau_{weak}/\tau_{strong}$: weak and strong ionization periods within one pulse; (3) τ_{off}/τ_{on}: voltage off/on times within the micro pulses; (4) f: pulse frequency; (5) P_a and P_p: average and peak target powers; (6) V_a and V_p: average and peak target voltages; (7) I_a and I_p: average and peak target currents; (8) I_d: peak ion current density on the target; (9) I_{sub}: substrate peak current density; (10) T_{sub}: average substrate temperature.

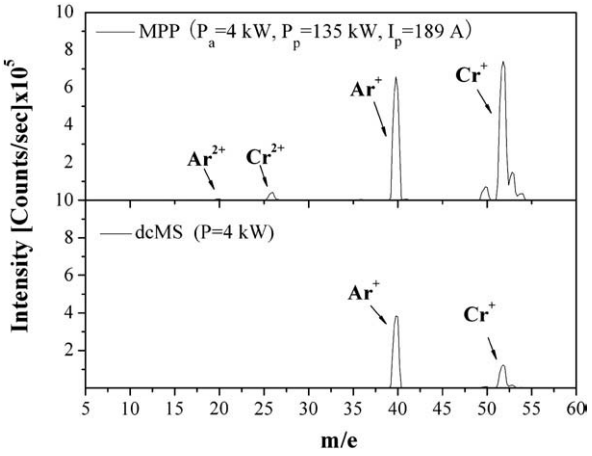

Fig. 2. Ion mass distributions of the dcMS and MPP plasmas generated at an average target power of 4 kW during sputtering of a Cr target in a pure Ar atmosphere.

growing film and will affect the grain growth kinetics, which may lead to the large grain growth in the (200) orientation.

On the other hand, all MPP Cr coatings exhibited a strong (110) orientation, indicating a different grain growth kinetics as compared to the dcMS Cr coatings when the average target power was higher than 2 kW. The coating thickness/deposition rate increased rapidly when the P_a was higher than 2 kW, as confirmed in the SEM observations. As compared to the dcMS Cr coatings deposited at similar P_a levels, it is evident that MPP Cr coatings exhibited denser microstructure and smaller grain size (Figs. 4 and 5). A comparison of the typical surface morphologies of dcMS and MPP Cr coatings is presented in Fig. 6. The dcMS coating deposited at 3 kW exhibited large crystals with the top grain size near 1 μm. However, the MPP Cr coating deposited at $P_a = 4$ kW, $P_p = 135$ kW and $I_p = 189$ A exhibited much smaller grains with a wide range of grain size distribution. The laminated feature of the grains indicates that the subgrain growth was significant in the MPP process, which is probably due to the high ion flux bombardment. This kind of surface feature is similar to the Nb coatings deposited using the ultra-high vacuum cathodic arc process, which is also an I-PVD process [19].

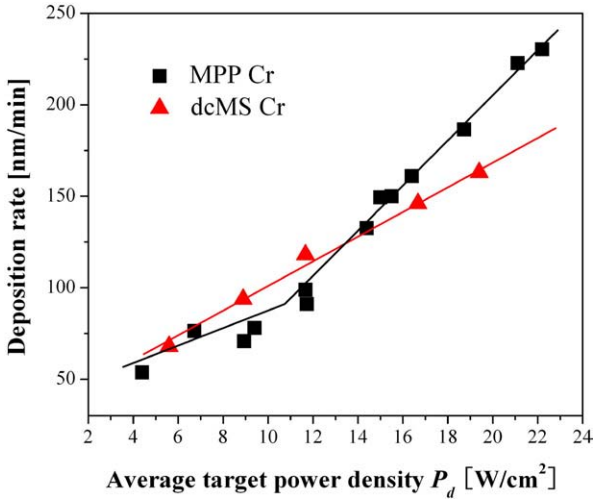

Fig. 3. Deposition rates of Cr coatings deposited using dcMS and MPP power sources as a function of the average target power density.

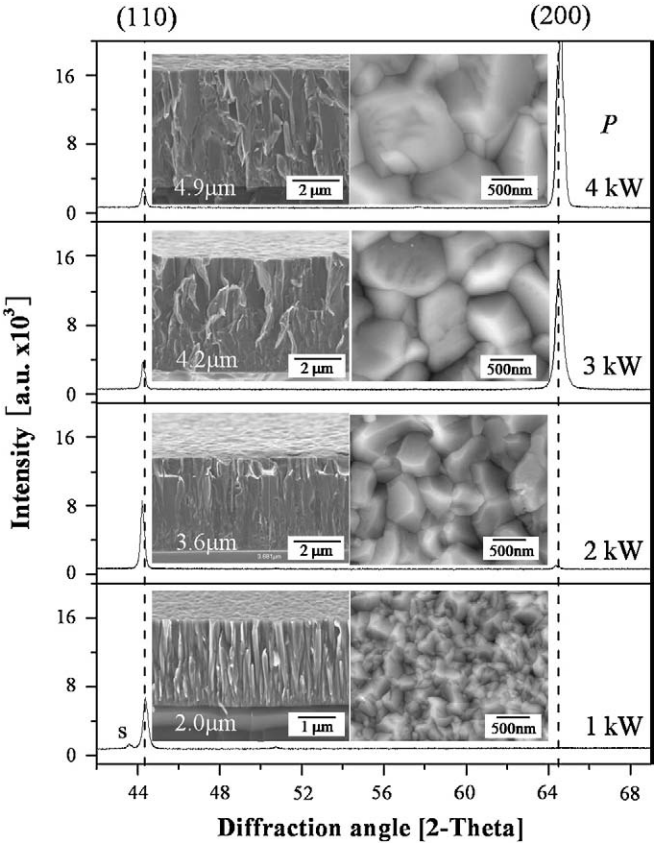

Fig. 4. XRD patterns and inserted SEM micrographs of the dcMS Cr coatings deposited at different target powers.

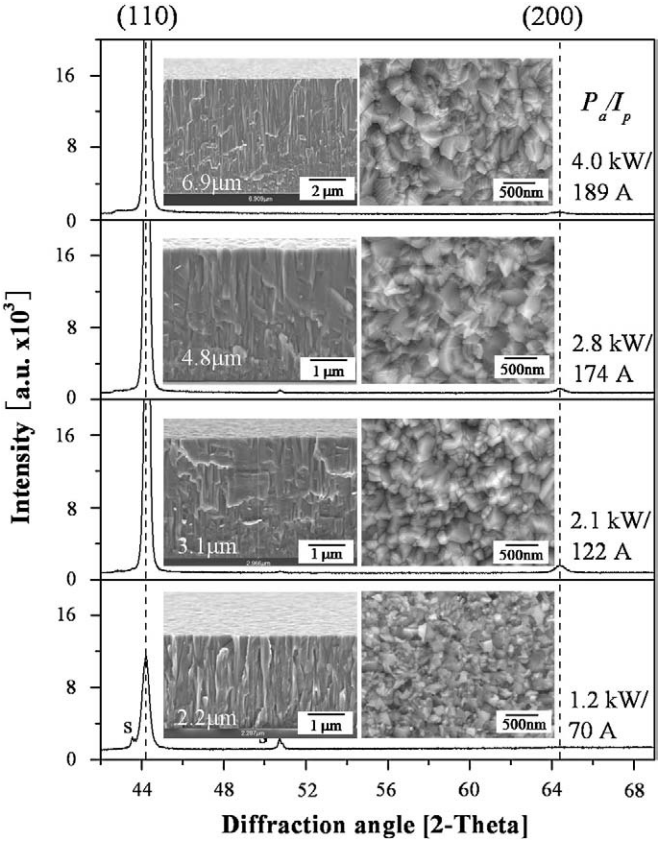

Fig. 5. XRD patterns and inserted SEM micrographs of the MPP Cr coatings deposited at different average powers and peak currents on the target.

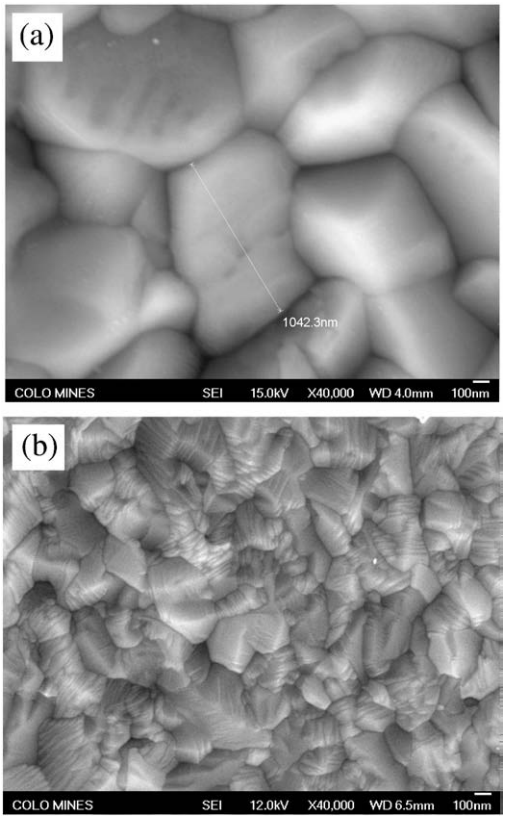

Fig. 6. Top view SEM micrographs of Cr coatings deposited in (a) dcMS (P = 3 kW) and (b) MPP (P_a = 4 kW, P_p = 135 W, and I_p = 189 A) conditions.

It has been shown that the MPP plasma exhibited significantly increased numbers of both Cr^+ and Ar^+ ions than the dc plasma at similar P_a (Fig. 2). Additionally, the ions in the MPP discharge showed a low peak ion energy at 1–2 eV and a small high ion energy tail (<30 eV) [16]. The substrate peak ion current density (I_{sub}), which is related to the number of ions arriving on the substrate, was measured in the MPP and dcMS conditions for similar average target powers, as shown in Fig. 7. The I_{sub} increased as the P_a was increased in both conditions. The I_{sub} exhibited low values of 2–5.5 mA cm^{-2} in the dcMS conditions, which

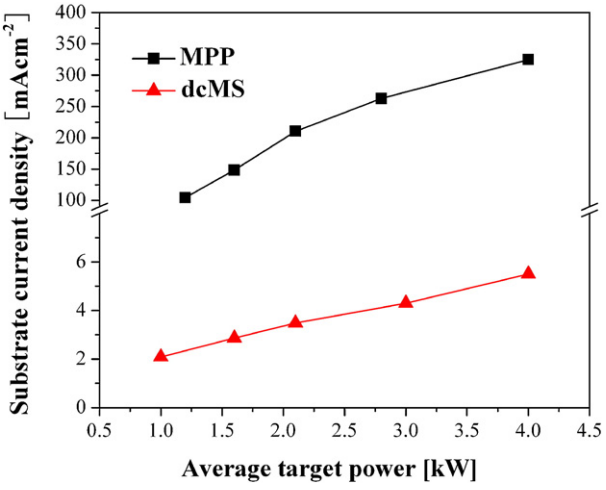

Fig. 7. The substrate peak current density measured in the MPP and dcMS conditions at similar average target powers.

agree with previous reported results for the dcMS in a closed field unbalanced magnetron sputtering configuration [20,21]. However, the I_{sub} significantly increased to 104–324 mA cm^{-2} in the MPP condition, which is more than 50 times higher than that found for the dcMS conditions. This result further confirmed that the number of ions arriving at the substrate in the MPP plasma is significantly higher than in the dcMS condition. Therefore, the highly ionized MPP plasma can provide extremely high ion flux bombardment on the growing film/substrate, thereby improving the coating density and decreasing the grain size as observed in the XRD and SEM studies (Figs. 5 and 6). Similar behaviors of the coating microstructure changes have also been observed for CrN films grown by HPPMS [1,22]. It is also interesting to find that the substrate temperatures in the MPP depositions are lower than in the dcMS conditions at equivalent target powers, as summarized in Table 1.

3.4. Mechanical and tribological properties

The hardness values of Cr coatings obtained by the two techniques are summarized in Table 1. The hardness of dcMS Cr coatings decreased from 8.9 to 4.2 GPa as the Cr target power was increased from 1 to 4 kW. The decrease in the hardness is probably due to the significantly increased grain size and change in the preferred orientation at high target powers. To the contrary, the hardness of MPP Cr coatings increased from 9 to 15 GPa as the target peak power and current were increased. The hardness enhancement in MPP Cr coatings is largely due to the fine grain size and improved coating density as compared to dcMS Cr coatings, as observed from the SEM micrographs (Figs. 4 and 5). The residual stresses of Cr coatings deposited using dcMS and MPP at a P_a of 3 and 2.8 kW respectively were measured by the $\sin^2\psi$ method using the X-ray diffractometer. It was found that the dcMS Cr coating has a low compressive residual stress of 0.5 GPa, whereas a higher compressive residual stress of 1.7 GPa was identified in the MPP Cr coating. The higher compressive residual stress observed in MPP Cr coatings may also contribute to the enhancement of the coating hardness by increasing the elastic energy stored in the coatings [23].

The adhesion of the dcMS and MPP Cr coatings was evaluated using the micro scratch test. The scratch track morphologies are illustrated in Fig. 8. As shown in Fig. 8a, for the dcMS Cr coating (P_a = 1.6 kW), the critical load for the first coating cracking (L_{C1}) was found to be as low as 2.8 N. Afterwards, massive continuous conformal cracks were observed within the scratch track together with some lateral cracks along the side of the track as the load was increased. The MPP Cr coatings showed improved adhesion. As shown in Fig. 8b, the MPP Cr coating deposited at P_a = 1.6 kW exhibited a higher L_{C1} at 5.1 N and much less conformal cracking as compared to the dcMS Cr coating. A further improved coating adhesion was achieved in the MPP Cr coating deposited at P_a = 4 kW and I_p = 189 A, in which a high L_{C1} of 12.5 N and a further decrease the number of conformal cracks in the track as is shown in Fig. 8c. Overall, all three Cr coatings showed excellent adhesion in that no coating chipping at the edge (L_{C2}) and coating delamination (L_{C3}) can be observed throughout the test.

There are two aspects should be considered to evaluate the adhesion strength of the Cr coatings. In general, there is an increase in the critical load with an increase in the coating thickness [24]. The thicker MPP Cr coating deposited at P_a = 4 kW (6.9 μm) will be more capable of distributing the applied force as compared to the thinner dc Cr coating deposited at P_a = 1.6 kW (2.8 μm). Laing et al. showed that a high I_{sub} achieved in the depositions is not only significant in producing dense coatings but also in the ion cleaning of the workpieces, which led to an increase in the coating adhesion [25]. The increased coating adhesion by sputter etching the substrate with highly ionized HIPIMS flux at a flux density approaching 300 mA cm^{-2} has also been reported by Ehiasarian et al. [26]. Therefore, it is assumed that the high I_{sub} obtained in the MPP Cr depositions (324 mA cm^{-2}) can provide enhanced low energy ion

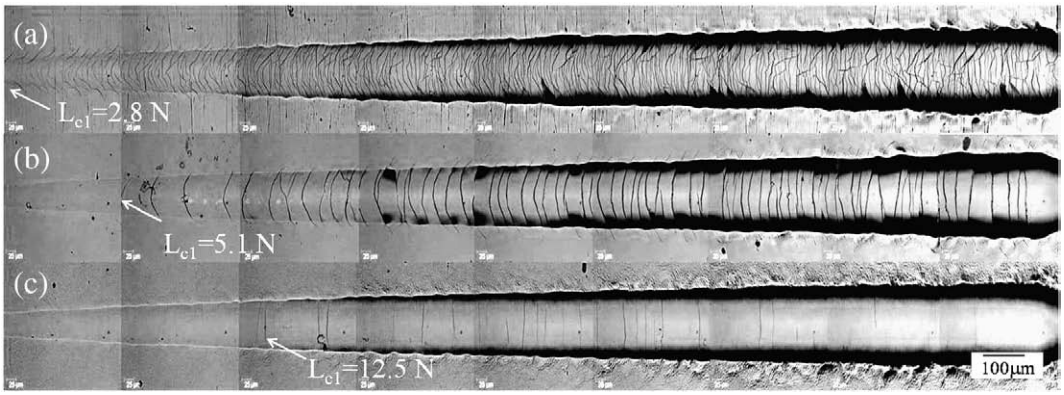

Fig. 8. Optical micrographs of the scratch tracks of the dcMS and MPP Cr coatings: (a) the dcMS Cr coating (P = 1.6 kW), (b) the MPP Cr coating (P_a = 1.6 kW, P_p = 65 kW, I_p = 94 A), and (c) the MPP Cr coating (P_a = 4 kW, P_p = 135 kW, I_p = 189 A).

bombardment at the beginning of the deposition to increase the adhesion strength between film and substrate atoms. However, further studies are needed to clarify the role of low energy ion bombardment on the interface strength and morphology during the MPP deposition.

4. Conclusions

Metal Cr coatings were deposited using MPP and dcMS in a closed field unbalanced magnetron sputtering system at similar average target powers. The ion mass scans confirmed a significant increase in the numbers of both target material and gas ions in the MPP plasma as compared to the dcMS plasma. The substrate peak current densities measured in the MPP depositions (104–324 mA cm^{-2}) have been increased by over a factor of 50 to that found for the dcMS conditions (2–5.5 mA cm^{-2}). It was found that MPP sputtering exhibits higher deposition rates than in the dc conditions when the average target power is above 14 W cm^{-2} for the Cr coating depositions. With the aid of the enhanced ion flux bombardment, MPP sputtered Cr coatings exhibited denser microstructure, smaller grain size, higher hardness and improved adhesion as compared to the dcMS Cr coatings.

Acknowledgement

We acknowledge the support of the MPP generator for the research program from the Zpulser, LLC, USA.

References

[1] A.P. Ehiasarian, P.Eh. Horsepian, L. Hultman, U. Helmersson, Thin Solid Films 457 (2004) 270.
[2] V. Kouznetsov, K. Macak, J.M. Schneider, U. Helmersson, I. Petrov, Surf. Coat. Technol. 122 (1999) 290.
[3] K. Macak, V. Kouznetsov, J.M. Schneider, U. Helmersson, I. Petrov, J. Vac. Sci. Technol., A, Vac. Surf. Films 18 (2000) 1533.
[4] U. Helmersson, M. Lattemann, J. Bohlmark, A.P. Ehiasarian, J.T. Gudmundsson, Thin Solid Films 513 (2006) 1.
[5] K. Sarakinos, J. Alami, C. Klever, M. Wuttig, Surf. Coat. Technol. 202 (2008) 5033.
[6] C. Reinhard, A.P. Ehiasarian, P.Eh. Hovsepian, Thin Solid Films 515 (2007) 3685.
[7] J. Alami, P.O.Å. Persson, D. Music, J.T. Gudmundsson, J. Bohlmark, U. Helmersson, J. Vac. Sci. Technol., A, Vac. Surf. Films 23 (2) (2005) 278.
[8] K. Bobzin, N. Bagcivan, P. Immich, S. Bolz, R. Cremer, T. Leyendecker, Thin Solid Films 517 (2008) 1251.
[9] M. Lattemann, A.P. Ehiasarian, J. Bohlmark, P.Å.O. Persson, U. Helmersson, Surf. Coat. Technol. 200 (2006) 6495.
[10] A. Anders, Phys. Status Solidi, A Appl. Res. 205 (4) (2008) 965.
[11] D.J. Christie, J. Vac. Sci. Technol., A, Vac. Surf. Films 23 (2) (2005) 330.
[12] J. Alami, K. Sarakinos, G. Mark, M. Wuttig, Appl. Phys. Lett. 89 (2006) 154104.
[13] S. Konstantinidis, J.P. Dauchot, M. Ganciu, A. Ricard, M. Hecq, J. Appl. Phys. 99 (2006) 013307.
[14] William D. Sproul, Roman Chistyakov, Bassam Abraham, Society of Vacuum Coaters News Bulletin, Summer 2006, p. 35.
[15] R. Chistyakov, U.S. Patent 7, 147, 759, "High-power pulsed magnetron sputtering", December 12, 2006.
[16] J. Lin, J.J. Moore, W.D. Sproul, B. Mishra, J.A. Rees, Z. Wu, R. Chistyakov, B. Abraham, Surf. Coat. Technol. 203 (2009) 3676.
[17] J. Vlcek, B. Zustin, J. Rezek, K. Burcalova, J. Tesar, 52nd Annual Technical Conference of the Society of Vacuum Coaters, paper HP-5, May 11 2009, Santa Clara, CA.
[18] S.M. Rossnagel, J. Hopwood, Appl. Phys. Lett. 63 (1993) 3285.
[19] J. Langner, M.J. Sadowski, P. Strzyzewski, R Mirowski, et al., XXIInd Int. Symp. on Discharges and Electrical Insulation in Vacuum, Matsue, 2006, p. 535.
[20] W.D. Sproul, P.J. Rudnik, M.E. Graham, S.L. Rohde, Surf. Coat. Technol. 43/44 (1990) 270.
[21] S.L. Rohde, I. Petrov, W.D. Sproul, S.A. Barnett, P.J. Rudnik, M.E. Graham, Thin Solid Films 193/194 (1990) 117.
[22] J. Alami, K. Sarakinos, F. Uslu, M. Wuttig, J. Phys., D, Appl. Phys. 42 (2009) 015304.
[23] W.R. Lafontaine, B. Yost, C.Y. Li, J. Mater. Res. 5 (1990) 776.
[24] W. Heinke, A. Leylan, A. Matthews, G. Berg, C. Friedrich, E. Broszeit, Thin Solid Films 270 (1995) 431.
[25] K. Laing, J. Hampshire, D. Teer, G. Chester, Surf. Coat. Technol. 112 (1999) 177.
[26] A.P. Ehiasarian, J.G. Wen, I. Petrov, J. Appl. Phys. 101 (2007) 054301.